International Journal of Robotics and Control Systems
Vol. 2, No. 2, 2022, pp. 408-423
ISSN 2775-2658
http://pubs2.ascee.org/index.php/ijrcs

Performance Analysis of PSO DFFP Based DC-DC Converter with Non Isolated CI using PV Panel

C. Nagarajan [1*], K. Umadevi [2], S. Saravanan [2], M. Muruganandam [3]

[1] Muthayammal College of Engineering, Rasipuram, TN
[2] Muthayammal Engineering College, Rasipuram, TN
[3] Department of Engineering, University of Technology and Applied Sciences – Ibri
[1] nagaraj2k1@gmail.com
*Corresponding Author

ARTICLE INFO

Article history
Received April 02, 2022
Revised April 28, 2022
Accepted June 15, 2022

Keywords
PSO-DFFP;
PV;
Power Converter;
Coupled Inductor (CI);
ANFIS

ABSTRACT

This article presents the modeling and development of a DC-DC converter with Partial Swarm Optimization with Distinctive Feed Forward Propagation (PSO-DFFP) controller for hybrid power systems, including photovoltaic panels. The transient and dynamic analysis of the proposed controller has been presented. The PSO-DFFP controller has been designed to improve the operating efficiency and reduces the input converter current ripple. The ANFIS and PSO DFFP controllers are developed, and the performance of the system is compared. The proposed system reduces the switching losses and voltage drops in switching modes. The proposed system is demonstrated and developed with a 200W, 100kHz model. From the experimental results, it can be exposed that the proposed system is acceptable for PV applications.

1. Introduction

As solar power is accessible in nature and exceptional in its unlimited availability, it has to turn into the majority of promising renewable sources. It has considered a recognizable source of low-cost renewable sources because it is low in operating costs and free of environmental issues. The costs of solar modules are high, and the generation of power using PV systems, especially grid-connected types, has been commercialized because of their inherent long-term benefits. However, photovoltaic power is not in the system. Module, Maximum Power Point Tracking (MPPT) usually works with a power converter (DC-DC converter and inverter) to improve the use of large arrays. Mostly, the energy demand is supplied using fossil fuels. However, the emerging problems such as increased air pollution vanishing of fossil fuels have made us migrate toward Renewable Energy Sources (RES), which can be used as an energy supplier. However, the power obtained from PV may be reduced due to partial shading and mismatch condition in town areas. At the same time, the low conversion efficiency of the PV system also makes it expensive [1].

Bei et al. [2] have developed and designed the high gain inter leveled converter with the solar panel using a sliding mode controller was presented. The controller performance of the converter was presented with simulation analysis. Stalin et al. [3] have described the soft switched bidirectional converter was designed with PI and a Fuzzy logic controller (FLC). The PI and FLC performance was described for the soft switched converter [4]. The controller performance was compared and tabulated.

Adib et al. [5] have designed the ultracapacitor batteries for the bidirectional soft switched converter was presented. The PWM control technique was presented with capacitor design analysis. The transient and dynamic analysis of the bidirectional converter was not presented.

Baggio et al. [6] have developed and demonstrated the isolated interleave ZVS converter was presented. The phase-shifted Pulse width modulation controller technique was designed and presented. The switch performance of the soft switched converter was presented. The converter performance was also analyzed with sliding mode control technology. The non-isolated buck voltage controller module with ZVS asymmetrical converter was presented [7-10].

Zhang et al. [11] have demonstrated the bidirectional soft switched DC/DC converter. Here, the converter is operated in full load, and thus the soft switched converter produced 98 percent of the converter efficiency. The ZVS-based bidirectional soft switch converter was controlled by phase shift pulse width modulation was presented [12-16]. Prasad et al. proposes a new photovoltaic system that consists of a DC / DC power converter and a new 7-level inverter. The proposed PV system is in phase with the utility voltage and produces a sinusoidal output current that is supplied to the utility. A prototype is developed and tested to confirm the performance of this proposed PV system. Rooftop photovoltaic systems mean that their generated power is not monitored and is not normally visible to system operators [17]. If a significant number of systems are installed, invisible photovoltaics can significantly alter the net load on the power system. In this method, a data-driven approach is proposed that uses a small number of measurements at a representative site to estimate invisible solar power generation.

Flexible loads such as Residential Air Conditioners (ACS) can be controlled to provide demand-side conditioning and balancing services directly in the electric grid [18]. Large agglomeration of AC provides resources similar to those of distributed energy storage systems that can be used to compensate for fluctuations in the power output of local renewable energy generation. This formulation directly and directly controls the aggregate demand of AC clusters in decentralized houses and decentralized and centralized Model Predictive Control (MPC) strategies for solar power balance fluctuations. Dynamic power flow management system for photovoltaic (PV) systems Dual input/output DC-DC converter using a single inductor-based single stage to supply a standalone DC load, backed up by a secondary battery [19-30].

The research contribution is to an analysis of the transient and dynamic performance of the DC/DC converter is important in high power applications. Hence the proposed PV-based soft switched DC-DC converter with a non-isolated coupled inductor has been implemented using a PSO-DEEP controller for estimating various performances. The overall performance and efficiency are improved by this method. This converter can produce a high efficiency under heavy load conditions. It can be applied in other types of converters such as dc-dc converters, regulators, and motor control applications. The transient and dynamic performance of the soft switched DC-DC converter is presented. A 200 W, 100 kHz prototype model of the converter is demonstrated, and the experiment results are analyzed and compared with the simulation results.

2. Proposed Soft Switched Converter

Fig. 1 explains the overall map of the proposed system. The proposed system consists of a PV array, PSO DFFP controller, boost converter, filter, and RLE load. The photovoltaic power creation system produces different voltages of temperature and luminosity. Two hundred sets of data simulate the data through various temperatures and lights. This data is also used by the MATLAB toolbar to use a Boost Converter for the purpose of the Maximum Power Point Monitoring (MPPT) PV line. The boosted voltage is given to the voltage source inverter. The inverter feeds the power to the three-phase ac load. The output voltage from the inverter is given to the LC filter to reduce the harmonic voltages in the load.

A boost converter can be used for a DC output that is not controlled by a controlled DC input to convert to the required volume volts. Its circuit diagram is shown in Fig. 2. They usually turn this voltage off, and then the stored energy is transferred to a DC voltage and transferred to a controlled voltage output during the current that causes the energy to flow across the inductor or transformer. The output voltage is controlled by adjusting the on/off time. This is achieved by using a power switch-mode circuit whose element dissipation is negligible. Pulse width modulation allows control and regulation of the total output voltage. It is considered the heart of electricity. Therefore, it can affect the overall performance of the power system.

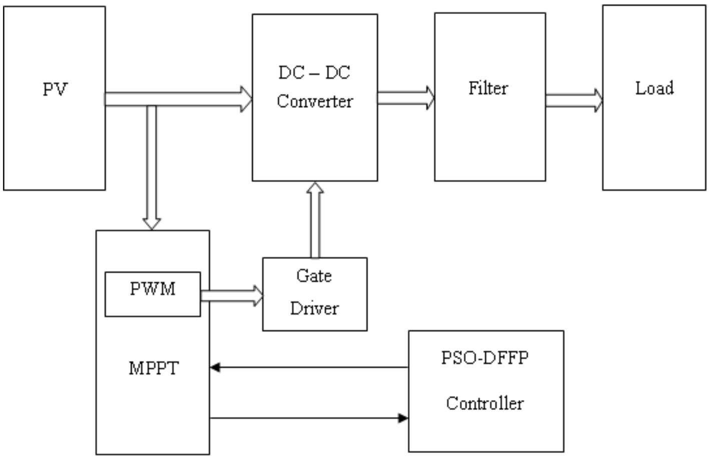

Fig. 1. Proposed Block Diagram PSO-DFFP System

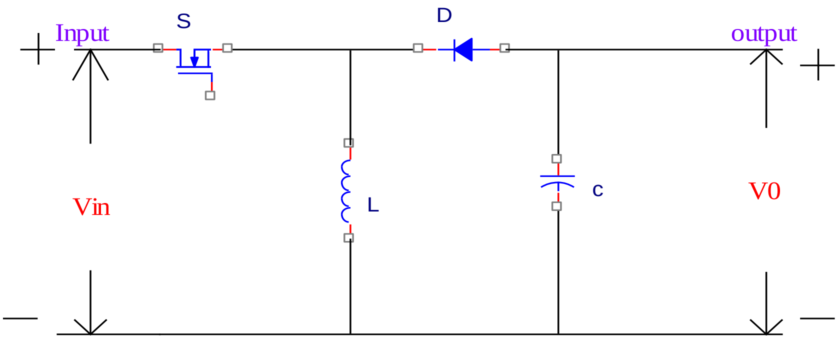

Fig. 2. Schematic diagram of the proposed DC/DC converter

When the MOSFET switch is in this state (off), the entire circuit is divided into two sides that are input to the input side of the output side. A closed loop containing a trigger input will cause the current to flow through the current circuit. This current will increase linearly until the switch is off. When the hen MOSFET switch is in this state (off), the entire circuit is divided into two sides that are input to the input side of the output side. The closed-loop is included in the input. At the same time interval, the high-inductance voltage is passed to any load but to itself. The diode is off during this mode. When the switch is in the (on) mute position, when the power is turned on, the inductor and RC, there will be a closed-loop and load when the power stored in the inductor is stored in the RC by the diode. Therefore, the capacitor charging in the current load region of the inductor decreases linearly.

Fig. 2 describes the working principle proposed DC-DC converter system. During the continuous conduction mode of operation, buck-boost converter, $V_L = V_{in}$ while the MOSFET is ON state when the MOSFET is off state, it can be expressed as $V_L = V_o$. For Zero net current changes over a period, the average voltage across the inductor is zero.

$$V_{in}t_{on} + V_o t_{off} = 0 \tag{1}$$

Which gives the voltage ratio

$$\frac{V_0}{V_{in}} = -\frac{Dt}{(1 - Dt)} \tag{2}$$

and the corresponding current rate

$$\frac{I_o}{I_{in}} = -\frac{(1-Dt)}{Dt} \tag{3}$$

Where V_{in} is the Input voltage, t_{on} is on time duration, V_o is the output voltage, t_{off} is OFF time duration, Dt is the Duty cycle ratio of the PWM modulation, and V_L is lin voltage.

MOSFET duty ratio (Dt) is between 0 and 1. During this time, the voltage of the converter is varied from low to higher magnitude. Mainly operating ranges of the inductor describe the limitation between the continuous and discontinued conduction modes, which is given by

$$L_1 = \frac{(1-Dt)^2}{2Dt} \tag{4}$$

However, a significant difference is the use of directional information in the current population distance to guide the DFFP search process. The DE performance depends on the operation of the target vector and the difference vector to obtain a test vector. The mutation is the main business in DFFP.

A mutant vector is generated by

$$X_i^{\prime G} = X_a^G + F(X_b^G - X_c^G) \tag{5}$$

Where $a \neq b \neq c \neq I$, $X_a^G X_b^G X_c^G$ is random vectors, F is a mutation factor with the range [0, 1]. Thus the general structure of a PSO-DFFPis depicted in Fig. 3.

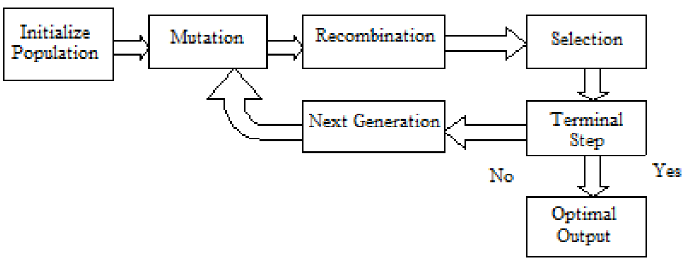

Fig. 3. General Structure of PSO-DFFP

3. Results and Discussion

3.1. Design of ANFIS Controller

ANFIS is an association of Fuzzy and Neural Networks (NN). In ANFIS, Neural Network learning methods improve the parameters of FIS. ANFIS network structures comprise five discrete layers and are depicted in Fig. 4. It comprises two inputs and one output.

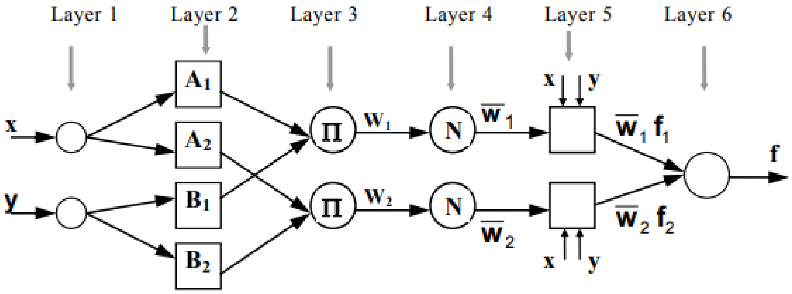

Fig. 4. The architecture of ANFIS (Two Inputs).

In Fig. 4, each circle and square represents a fixed node and an adaptive node, respectively. The rule base of this system has two if-then rules (Takagi-Sugeno'stype) and are depicted as

$$\begin{array}{lll} \text{Rule 1:} & \textit{if } y_1 \textit{ is } A_1 \textit{ and } y_2 \textit{ is } C_1; & \textit{then } z_1 = a_1y_1+b_1y_1+c_1 \\ \text{Rule 2:} & \textit{if } y_1 \textit{is } A_2 \textit{ and } y_2 \textit{ is } C_2; & \textit{then } z = a_2y_1+b_2y_2+c_2 \end{array} \tag{5}$$

and its function is stated as follow.

Layer 1
All the nodes of this layer are considered input nodes, and through this, externally applied signals are conveyed to other layers.

Layer 2
In layer 2, a generalized bell membership function is implemented, and its degree is calculated as follows.

$$\mu_A(x) = gbell(x; a_i, b_i, c_i) = \frac{1}{1 + \left|\frac{x_i - c_i}{a_i}\right|^{2b}}$$

Where $a_{i,}\, b_{i,}\, c_i$ is factor set, c is the center of the function, a is Half of the width, and b is controlling the slopes at the crossover points.

Layer 3 (Fuzzification Layer)
The output obtained from this layer is the artifact of all the input signals.

$$w_i = \mu A_i(x)\mu B_i(y), i = 1,2$$

Layer 4
Here, each node computes its own firing strength. It is the proportion of the firing strength of i^{th} rule to the summation of firing strengths of the whole rule.

$$\overline{w}_i = \frac{w_i}{w_1 + w_2}, i = 1,2$$

The output obtained in the layer is called normalized weight.

Layer 5
The nodes in this layer are adaptive in nature with a node function.

$$\overline{w}_i fi = \overline{w}_i (p_x + q_i y\_r_i)$$

$\overline{w}_i$ is normalized weight from layer 3

Layer 6
A node that is present under this layer calculates the output.

$$Overall\ output = \Sigma_i \overline{w}_i fi = \frac{\Sigma_i w_i fi}{\Sigma_i w_i}$$

Thus the design of an ANFIS controller implemented here is discussed above, and thus the fuzzifier comprises two inputs, namely, the error signal (e) / change in error signal (ce). The Gaussian membership function is chosen as the Membership function. Thus they are characterized into seven functions and are tabulated in Table 1. Thus inputs to the ANFIS controller are fuzzified by utilizing a fuzzy set. Thus the rule base includes 49 (IF-THEN) rules.

Finally, NN is utilized for choosing the appropriate rule. Once an appropriate rule is labeled, a control signal required to obtain the optimum output is generated. Thus the defuzzifier section consists of a signal which can be able to control the switching states of the converter switches, the input neurons, viz., the change in error and error, influence the hidden layer of NN. Thus, in this proposed methodology, an optimum rule is obtained at the 4th-order hidden layer. Hence, 4 hidden layers are chosen in this work. Thus the defuzzified output is considered an output neuron. This defuzzified output generates the firing pulse of the converter. Fig. 5 shows the ANFIS training Flowchart of the controller.

Table 1. Fuzzy Rules

Δe/e	**NBig**	**NMed**	**NSma**	**ZE**	**PSma**	**PMed**	**PBig**
NBig	NBig	NBig	NBig	NMed	NMed	NSma	ZE
NMed	NBig	NBig	NMed	NSma	NSma	ZE	PSma
NSma	NBig	NMed	NSma	NSma	ZE	PSma	PMed
ZE	NMed	NSma	NSma	ZE	PSma	PSma	PMed
PSma	NMed	NSma	ZE	PSma	PSma	PMed	PBig
PM	NSma	ZE	PSma	PSma	PMed	PBig	PBig
PBig	ZE	PSma	PMed	PMed	PBig	PBig	PBig

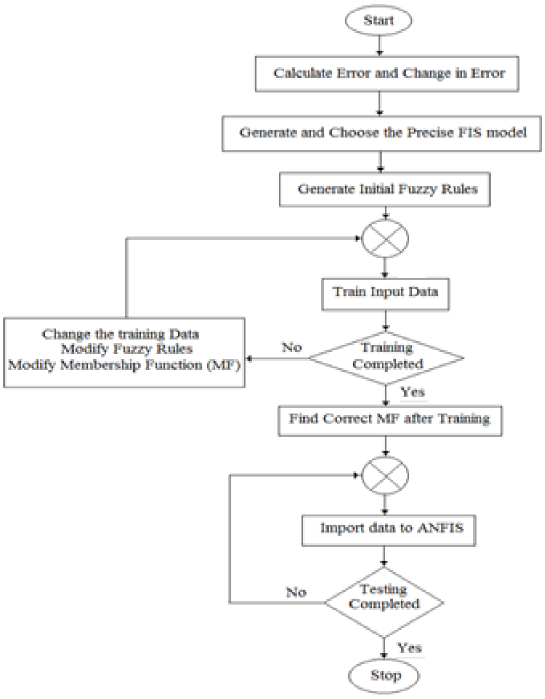

Fig. 5. ANFIS training Flowchart

3.2. Design of PSO-DFFP Controller

Parameters of the Soft Switched Converter with Coupled Inductor values are designed [22] as shown in Table 2.

Table 2. Simulation Parameters

Parameters	**Output**
Maximum Power	200Watts
Switching Frequency	100kHz
Short circuit voltage	80v
Current at maximum power	5.29A
Short circuit Current	5.29A
Open circuit Voltage	38.5V
Inductor	100µH
Turns ratio	3
Capacitors	10µF
Output capacitor	47µF

The mechanism of PSO-DFFP is inspired by the complex social behavior shown in Fig. 6. For a D-dimensional search space, the position of the ith particle is represented as Xi = (xi1, xi2, xiD). Each particle controls a memory of its previous best position Pi = (pi1, pi2… piD) and a velocity Vi = (vi1, vi2…viD) along each dimension. In each iteration, the P vector in the particle with the best fitness near the local, specified grams and the current particle vector P is combined with the speed adjustment along each dimension, and the new position of the particle is found using that speed. The two basic equations that govern the work of PSO are the velocity vector and the position vector given by:

$$V_i^{(t+1)} = \omega \times V_i^{(t)} + c_1 \times r_1 \times \left(P_i^{best} - X_i^{(t)}\right) + c_2 \times r_2 \times \left(G^{best} - X_i^{(t)}\right) \tag{6}$$

where, $x_i^{(t)}$ is the present position of the particle i at iteration t, t is the Iteration pointer, p_i^{best} is the best position of the particle i until iteration t, G^{best} is the global best position of the entire swarm until iteration t, c_1 and c_2 is the acceleration coefficients vary between 0 and 4, $v_i^{(t)}$ is the velocity between the step size x_i^t and $x_i^{(t+1)}$, ω is the inertia weight/damping factor, which decreases from 0.9 to 0.4, used to control the contact of the new velocity with its previous velocity, r_1 and r_2 is Random variables with a range of [0, 2].

The following equation calculates the inertia weight ω.

$$\omega = \omega_{max} - \frac{\omega_{max} - \omega_{min}}{iter_{max}} \times iter \tag{7}$$

where, ω_{max} is initial weight, ω_{max} is the final weight, $iter_{max}$ is maximum iteration number, $iter$ is the current iteration number.

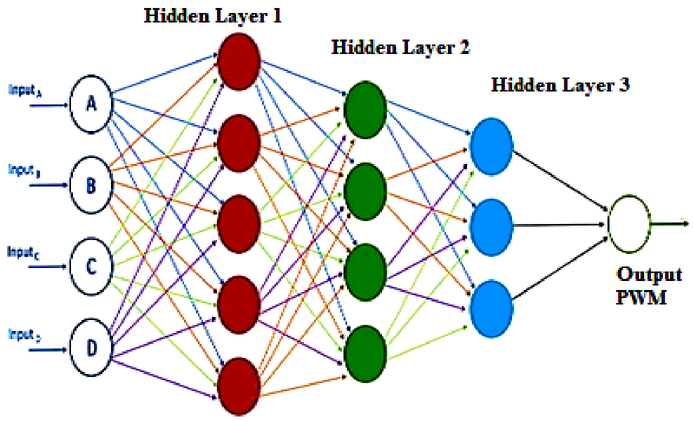

Fig. 6. Hybrid PSO-DFFP trained network

A new velocity is calculated in the direction of Pi^{best} and G^{best} to execute a change in the current search point. Every particle attempts to migrate from its current position to the new position by using the modified velocity given below in the equation

$$X_i^{(i+1)} = X_i^{(t)} + V_i^{(t+1)} \tag{8}$$

3.3. Proposed PSO-DFFP

It started as a usual particle swarm algorithm, and we found the speed of the swarm particles as given in below. Then we find a more advantageous position from the current particles and the updated position. Then it will cross and select according to the PSO-DFFP rules. Continue this process until you stop certain conditions from being met,

Step 1: Initialize random population
Step 2: Set the initial velocity of each particle equal to zero.
Step 3: Find velocity by using PSO-DFFP
Step 4: Find a new position
Step 5: Select the fittest location

Step 6: Perform mutation and crossover
Step 7: Repeat steps 2 to 7 until some stopping criteria are met.

Step 1: Start the training process

Step 2: The inputs at this stage are temperature, load, and PV production. This task will continue until enough data has been collected to complete offline training.

Step 3: Set the connection right between the input node and the output node. The range of typical domains can be obtained directly from previous requirements or determined from DFFP training data as follows:

$$w_{kj}^{L} = min\{x_{kj}^{K}\} \tag{9}$$

$$w_{kj}^{u} = max\{x_{kj}^{K}\} \tag{10}$$

Step 4: Obtain the forecasted data.

Step 5: Calculate the first cluster center of every cluster.

$$\begin{gathered} Z_k = \{z_{k1}, z_{k2}, \dots, z_{kn}\} \\ z_{kj} = \frac{w_{kj}^{L} + w_{kj}^{U}}{2} \; for\; k = 1,2 \dots n_c; j = 1,2, \dots n \end{gathered} \tag{11}$$

Step 6: Read the i^{th} training pattern and its cluster number p.

$$X_i^p = \{x_{i1}^p, x_{i2}^p, \dots, x_{in}^p\}, p \in n_c \tag{12}$$

Step 7: Use the proposed technique to calculate the distance between the training pattern X_i^p and the k^{th} cluster as follows:

Step 8: Upgrade the weights of the p^{th} and the k^{*th}clusters as follows:

(a) Upgrade the centers of the p^{th} and the k^{*th} clusters.

$$Z_{pj}^{new} + \eta\left(x_{ij}^{p} - z_{pj}^{old}\right) \tag{13}$$

(b) Up the weights of the p^{th} and the k^{*th} clusters.

Step 9: Repeat steps 3 to 6. If all patterns have been classified with PSO-DFFP, then the epoch of learning is over.

Step 10: Stop if the clustering process has converged and the total error rate has reached a predetermined value; otherwise, return to step 3.

The converter reaches its steady-state voltage output in 0.2 ms. However, for MPPT operation, voltage and current measurement intervals are set to 20 ms to avoid unnecessary noise from the entire electric circuit. The proposed PSO-DFFP operation should control the converter switching pulse in order to have maximum tracking accuracy and minimum overall tracking time. Fig. 7 shows the PSO-DFFP training Flowchart of the controller.

Fig. 7 represents the PSO DFFP controller design which generates gate pulse generation for switches. The comparator compares the reference voltage with the actual output voltage, and the difference in voltage is given to the controller. Then the controller produces a pulse to switch to minimize the error.

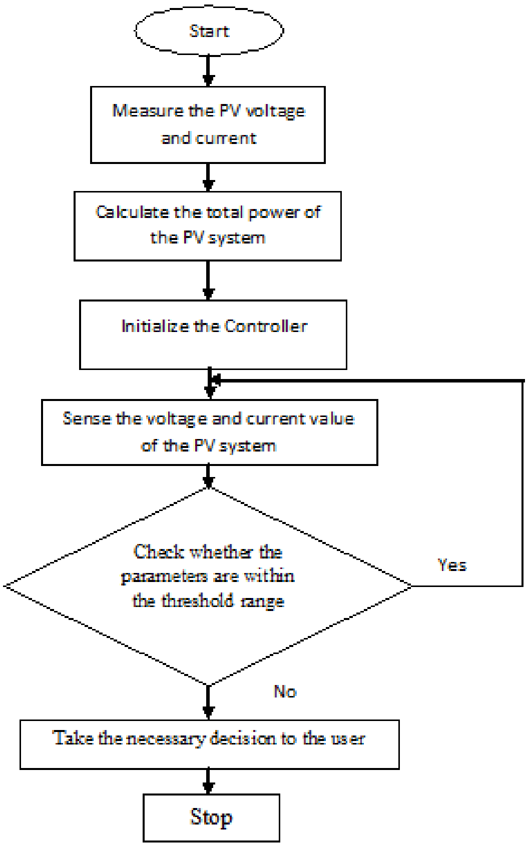

Fig. 7. PSO-DFFP training Flowchart

4. Simulation Results

This proposed PSO-DFFP-based MPPT method utilizing MATLAB2017a software is to be used and simulate the system (Fig. 8). The photovoltaic module is characteristic of the effect of the partial shadow state utilizing an arbitrary source to form a series of attached photovoltaic cells with radiation. The temperature of the photovoltaic module is kept constant at 25°C during the simulation. The shadow-free voltage module has a radiation-considerable exterior at 1000W/m2. The radiation on the marked voltage block is changing beyond the standard from 0 to 1000W/m2. As cycles of duty are reinitialized for each shift in radiation medicine, fast-tracking speeds and nearly zero latency fluctuations in MPP are achieved from computing power; Duty cycles will be updated according to the proposed technique.

Fig. 9 shows the output voltage/current of the proposed soft switching converter with a coupled inductor for sudden line disturbances at rated supply is presented with various controllers. The ANFIS settled at 0.00084 sec with refusal overshoot and settled at 0.0015 seconds amid line supply unsettling influence. Additionally, The PSO DFFP settled at 0.0006 seconds without oscillations, and good transient and dynamic performance for and in line disturbances system settled at 0.0009 seconds. The PSO DFFP Controller performed well compared to other controllers.

From the results made for the purpose of comparison, it was determined that the PSO DFFP controller is more effective and faster than the other controllers. The PSO DFFP controller reaches the reference value faster and is less affected by load changes. As seen from the Figures, it is concluded that the output voltage Vo is kept almost constant under large input voltage or load changes under the PSO DFFP controller.

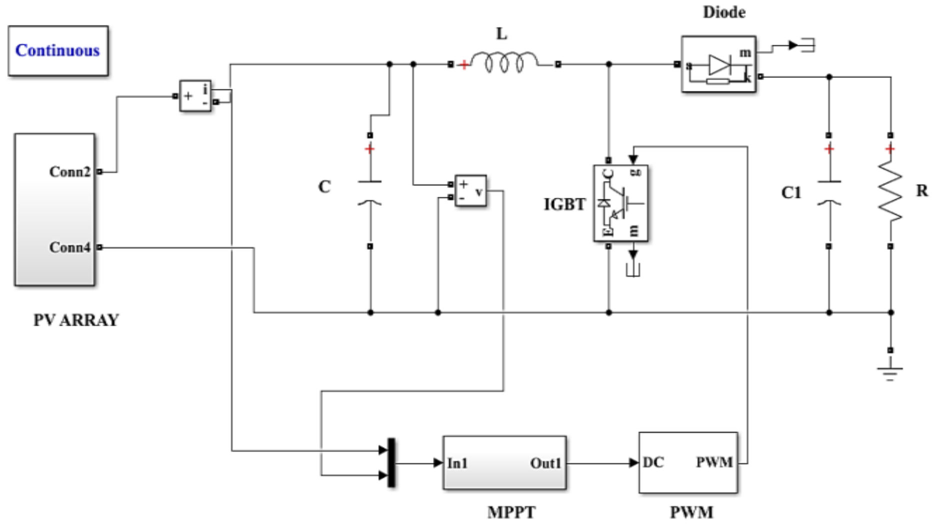

Fig. 8. Closed-loop Simulink model of the proposed converter

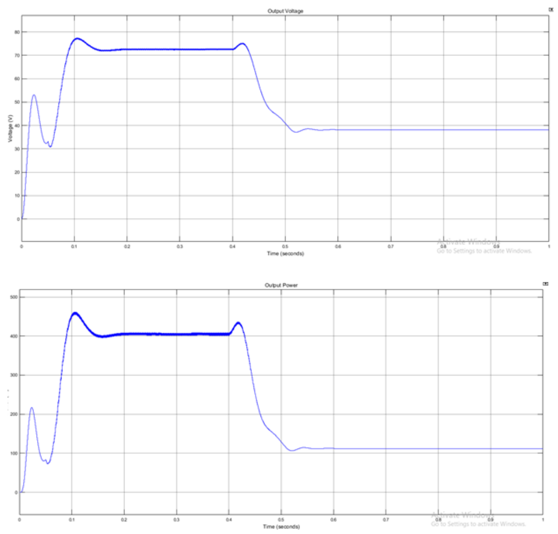

Fig. 9. Simulated results of voltage, current, and power tracked using the proposed PSO-DFFP algorithm for variation in irradiation condition

Fig 10 shows the Output Voltage and Current of the proposed system for under load disturbance attained in 0.06Sec and 0.08Secat rated load is presented with different controllers. It is clearly seen in Fig. 10 that the proposed controller performed well in the load disturbances condition. The settling time and overshoot are very less while the converter is operated in the PSO DFFP controller. The proposed controller produced with less overshoot and without steady-state error during the load disturbances period.

The steady-state and converter performance of the controller is offered in Table 3. It is clearly shown that the proposed PSO DFFP controller produced a rapid settling time and zero percentage overshoot compared to the other controllers. The rise time is 0.4, and the steady-state error is 0.0001.

Table 3. Steady-State Performance of the converter

Controller	Settling Time in Seconds	Steady-state error	Rise time in seconds	% Overshoot	THD in %
ANFIS	0.0009	0.001	0.59	0	6.8
PSO-DFFP	0.0006	0.0001	0.4	0	5.2

Vol. 2, No. 2, 2022, pp. 408-423

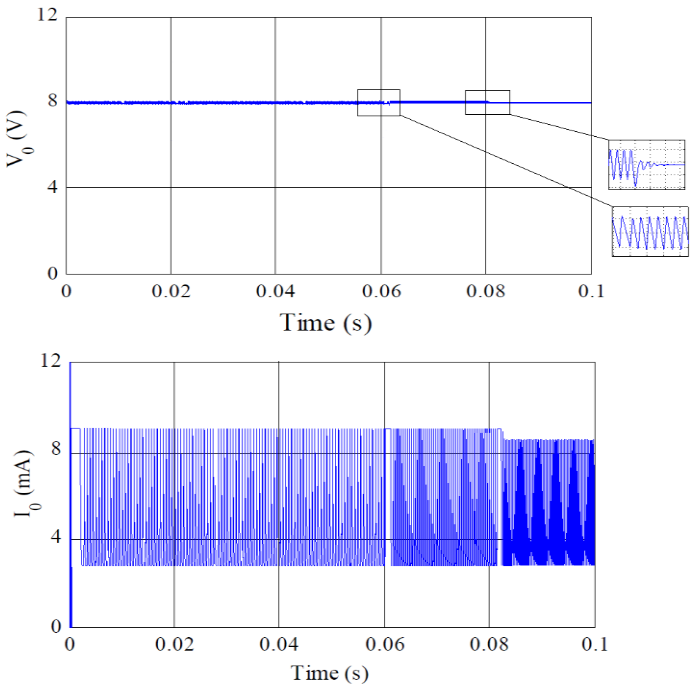

(a)

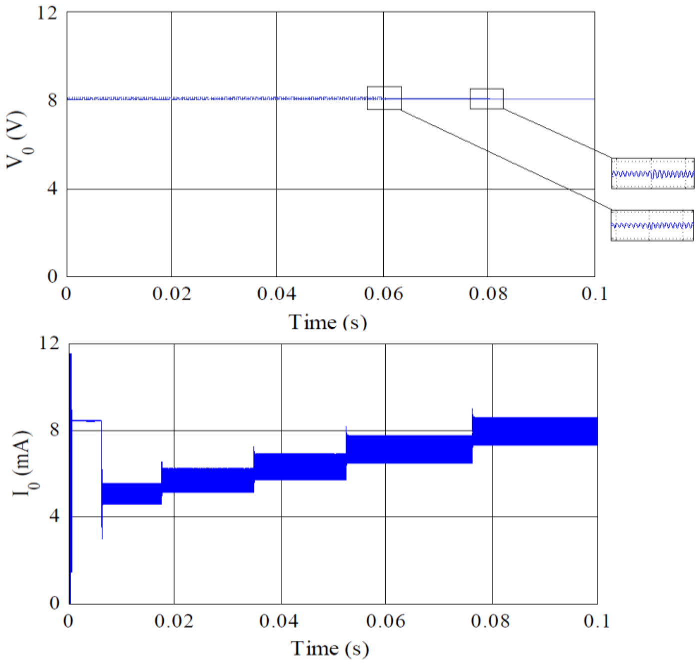

(b)

Fig. 10. Output Voltage and Current under Load Disturbance (a) ANFIS (b) PSO-DFFP Controller in 0.06Sec and 0.08Sec.

The Line disturbance and Load disturbance of the proposed system were performed in 0.06 and 0.08 sec, respectively. The performance of the controller underneath Line disturbance and Load disturbance is in Table 4 and Table 5, respectively. It is clearly absorbed from Table 4 the proposed PSO DFFP controller performed glowing in all supply disturbance conditions. The proposed PSO DFFP controller produced a very less percentage overshoot and quick settling time compared to the ANFIS Controller. Thus the proposed system is operated in different load disturbance conditions, and it is tabulated in Table 5. The PSO DFFP controller created the overshoot is 0.00001 percent, and the settling time is 0.018 in full load condition. The table result justifies that the percentage overshoot, rise time, and settling time of output voltage in ANFIS is more than the proposed PSO DFFP controller. It can be clearly seen that the overshoot and the settling time (t_s) are very low, and the response has less oscillation compared to other controllers.

Table 4. Performance of the proposed system under Line Disturbance

Controllers	Line Disturbance 25% at rated supply		Line Disturbance at 50% at rated supply		Line Disturbance at 100% at rated supply	
	Settling time (second)	% overshoot	Settling time (second)	% overshoot	Settling time (second)	% overshoot
ANFIS	0.012	0.0001	0.016	0.0001	0.017	0.0001
PSO-DFFP	0.010	0.00001	0.015	0.00001	0.016	0.00001

Table 5. Performance proposed system under Load Disturbance.

Controllers	Load Disturbance 25% rated Load		Load Disturbance 50% rated Load		Load Disturbance 100% rated Load	
	% overshoot	Settling time in (second)	% overshoot	Settling time in (second)	% overshoot	Settling time in (second)
ANFIS	0.0001	0.015	0.0001	0.018	0.0001	0.019
PSO-DFFP	0.00001	0.014	0.00001	0.017	0.00001	0.018

4.1. Experimental Setup

The solar panel-based soft switching converter with coupled inductor model is implemented, and the performance of the system experiments. A prototype proposed converter with PSO-DFFP controller is operating with 200W, 100kHz is designed and demonstrated. The P89V51RD2BN advanced microcontroller is used to generate the Pulse Width Modulation pulse signals, and IRFP940 MOSFET with heat sink is used as soft switched converter Q1 and Q2 Switches. In the MUR4100, diodes are used in the converter circuit and freewheeling. The 100kHz operating frequency is received from the generated pulses unit. The opt coupler CYN 19-1 generates the driving PWM pulse from the P89V51RD2BN through the isolator, and the driver IC IR4110is used in the circuit. The output voltage can be controlled from the PSO DFFP controller output. The output voltage is measured using a digital pulse sensor numbered GP1L53V. The driving PWM pulse is given to ALM2907 voltage regulator IC, and the P89V51RD2BN controller receives the feedback signal from ADC0808CCN type ADC IC. The prototype models for the proposed converter with solar panels are represented in Fig. 11.

Fig. 11. Experimental setup

The output voltage and current of the proposed operation with different controllers are presented in Fig. 12 and Fig. 13, respectively, during line and load disturbance in 0.06sec. It is clearly seen in Fig. 13 that the proposed controller performed better and produced less settling time, steady-state error, and overshoot compared to the other converters. The other controllers created more oscillation and high overshoot in full load disturbance conditions. The Hardware Performance analyses of a converter with different controllers are tabulated in Table 6. The tabulation concluded that the proposed controller produces less oscillation during line and load disturbance conditions and formed better performance compared to the other controllers.

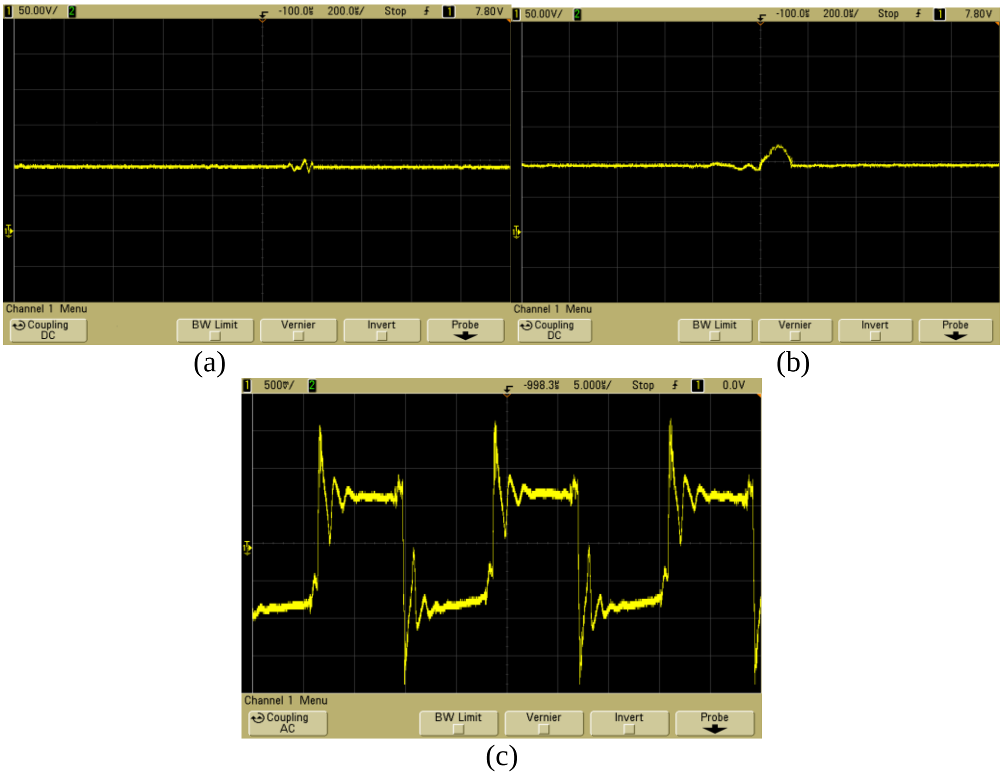

Fig. 12. Output voltage and current using ANFIS controller (a) Line disturbance (b) Load disturbance (c) output current in full load disturbance (disturbance in 0.06sec).

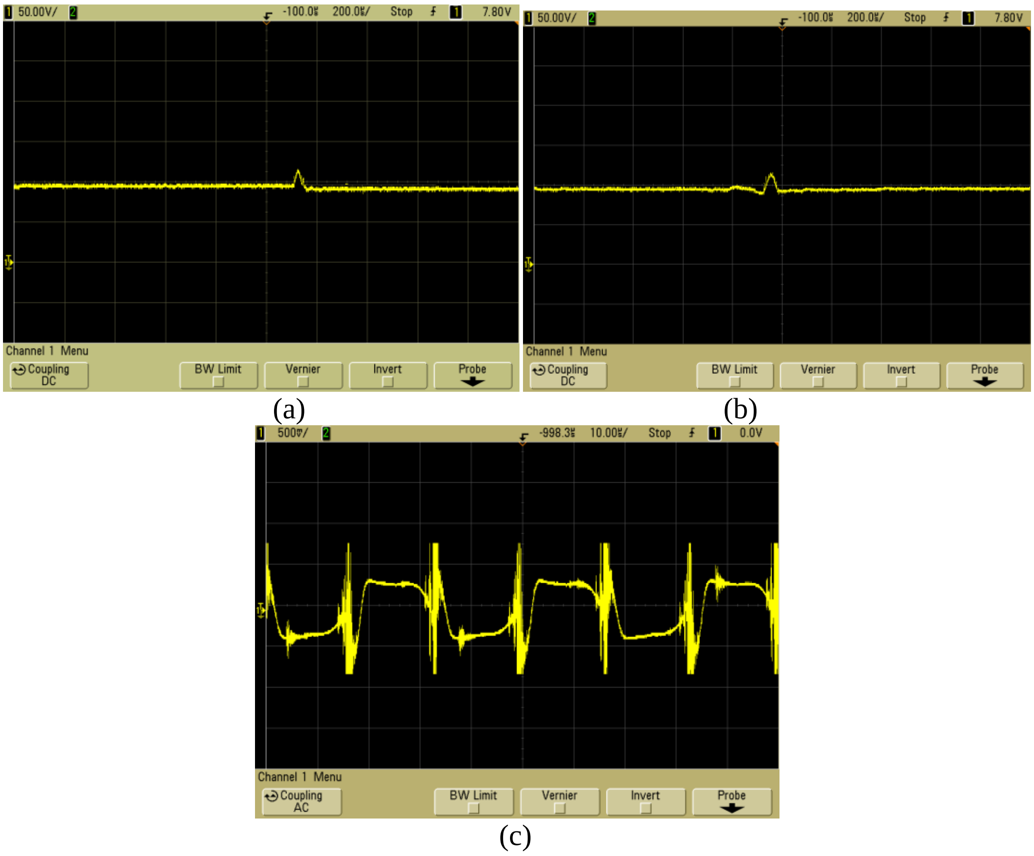

Fig. 13. Output voltage / current using PSO DFFP controller (a) Line disturbance (b) Load disturbance (c) output current in full load disturbance (disturbance in 0.06sec).

Table 6. Experimental analysis

Controller	Overshoot (%)	Rise time (t_s) in seconds	Steady state error I (AE)	Settling Time (t_s) in seconds
ANFIS	0.9	0.89	0.12	0.8
PSO-DFFP	0.84	0.72	0.1	0.6

5. Conclusion

The proposed PSO DFFP controller can be compared with the ANFIS controller and estimated with Simulink/ MATLAB tool. The mathematical form of the proposed converter has been considered and simulated with a different controller and estimated the performance for line disturbance and load disturbance conditions. It is fulfilled that the proposed controller gives a better transient and dynamic performance. A prototype 200W, 100 kHz converter was developed and demonstrated. The hardware results closely agree with the simulated results. In the future, the Fragmentary Power Prediction Algorithm (FPPA) will be developed and compared to the PSO DEEP.

Author Contribution: All authors contributed equally to the main contributor to this paper. All authors read and approved the final paper.

Funding: This research received no external funding.

Conflicts of Interest: The authors declare no conflict of interest.

Reference

[1] B. Gu, J. Dominic, J-S. Lai, Z. Zhao, and C. Liu," High Boost Ratio Hybrid Transformer DC-DC Converter for Photovoltaic Module Applications" *IEEE Transactions on Power Electronics*, vol. 28, no. 4, pp. 2048-2058, 2013, https://doi.org/10.1109/TPEL.2012.2198834

[2] T. Bei, P. Wang, L. Yang, and Z. Zhou, "Dynamic Sliding Mode Evolution PWM Controller for a Novel High-Gain Interleaved DC-DC Converter in PV System," *Journal of Applied Mathematics*, vol. 2014, pp.1-11, 2014, https://doi.org/10.1155/2014/658674

[3] B. Stalin and T. S. Sivakumaran, "Performance Evaluation of Bidirectional Soft switching Converter with Implementation of PI and Fuzzy Logic Controllers," *International Journal of Advanced Engineering Technology*, vol. 7, no. 3, pp. 42-53, 2016, http://www.technicaljournalsonline.com/ijeat/VOL%20VII/IJAET%20VOL%20VII%20ISSUE%20III%20JULY%20SEPTEMBER%202016/20167310.pdf.

[4] H. F. Farahani, "Designing and implementation of a fuzzy controller for DC-DC converters and comparing with PI digital controller," *Australian Journal of Basic and Applied Sciences*, vol. 5, no. 7, pp. 276-285, 2007, http://citeseerx.ist.psu.edu/viewdoc/download?doi=10.1.1.1077.9347&rep=rep1&type=pdf.

[5] E. Adib and H. Farzanehfard, "Soft switching bidirectional DC-DC converter for ultra capacitor batteries interface," *Energy Conversion and Management*, vol. 50, no. 12, pp. 2879-2884, 2009, https://doi.org/10.1016/j.enconman.2009.07.001.

[6] J. E. Baggio, H. L. Hey, H. A. Grundling, H. Pinheiro, and J. R. Pinheiro, "Isolated interleaved phase shift PWM DC-DC ZVS converter," *IEEE Transactions on Industry Applications*, vol. 39, no. 6, 2018, pp. 1795-1802, https://doi.org/10.1109/TIA.2003.818965.

[7] J. B. Banu and M. B. Moses, "Soft Switching Bidirectional Buck Boost Converter with Simple Auxiliary Circuit," *Indian Journal of Science and Technology*, vol. 9, no. 48, 2016, https://doi.org/10.17485/ijst/2016/v9i48/98037.

[8] K H. Cheng, C. F. Hsu, C. M. Lin, T. T. Lee, and C. Li, "Fuzzy neural sliding mode control for DC-DC converters using asymmetric Gaussian membership functions," *IEEE Transactions on Industrial Electronics*, vol. 54, no. 3, pp. 1528-1536, 2017, https://doi.org/10.1109/TIE.2007.894717.

[9] A. Balestrino, A. Landi, and L. Sani, "Cuk converter global control via fuzzy logic and scaling factors," *IEEE Transactions on Industry Applications*, vol. 38, no. 2, pp. 406-413, 2002, https://doi.org/10.1109/28.993162.

[10] Z. Zhang, W. Eberle, Y. F. Liu, and P. C. Sen, "A nonisolated ZVS asymmetrical buck voltage regulator module with direct energy transfer," *IEEE Transactions on Industrial Electronics*, vol. 56, no. 8, pp. 3096-3105, 2009, https://doi.org/10.1109/TIE.2009.2023102.

[11] J. Zhang, J. S. Lai, R. Y Kim, and W. Yu, "High-Power Density Design of a Soft-Switching High-Power Bidirectional DC-DC Converter," *IEEE Transactions on Power Electronics*, vol. 22, no. 4, 2007,pp. 1145-1153, https://doi.org/10.1109/TPEL.2007.900462.

[12] H. Xiao and S. Xie, "A ZVS Bidirectional DC-DC Converter with Phase-Shift Plus PWM Control Scheme," *IEEE Transactions on Power Electronics*, vol. 23, no. 2, pp. 813-823, 2008, https://doi.org/10.1109/TPEL.2007.915188.

[13] D. Liu and H. Li, "A ZVS bi-directional DC-DC converter for multiple energy storage elements," *IEEE Transactions on Power Electronics*, vol. 21, no. 5, pp. 1513-1517, 2006, https://doi.org/10.1109/TPEL.2006.882450.

[14] J. S. Prasad, Y. P. Obulesh, and C. S. Babu, "FPGA (Field Programmable Gate Array) controlled solar based zero voltage and zero current switching DC-DC converter for battery storage applications," *Energy*, vol. 106, pp. 728-742, 2016, https://doi.org/10.1016/j.energy.2016.03.002.

[15] C. Nagarajan and M. Madheswaran, "Stability Analysis of Series Parallel Resonant Converter with Fuzzy Logic Controller Using State Space Techniques," *Electric Power Components and Systems*, vol. 39, no. 8, pp.780-793, 2011, https://doi.org/10.1080/15325008.2010.541746.

[16] C. Nagarajan and M. Madheswaran, "Performance Analysis of LCL-T Resonant Converter with Fuzzy/PID Using State Space Analysis," *Electrical Engineering*, vol. 93, pp. 167-178, 2011, https://doi.org/10.1007/s00202-011-0203-9.

[17] S. Sathish Kumar and C. Nagarajan "Performance - Economic and Energy Loss analysis of 80 KWp Grid Connected Roof Top Transformer less Photovoltaic power Plant," *Circuits and Systems Journal*, vol. 7, no. 6, pp. 662-679, 2016, https://doi.org/10.4236/cs.2016.76056.

[18] C. Nagarajan and M. Madheswaran, "Experimental verification and stability state space analysis of CLL-T Series Parallel Resonant Converter with fuzzy controller," *Journal of Electrical Engineering*, vol. 63, no. 6, pp. 365-372, 2012, https://doi.org/10.2478/v10187-012-0054-2.

[19] C. Nagarajan, M. Muruganandam and D. Ramasubramanian, "Analysis and Design of CLL Resonant Converter for Solar Panel-Battery systems," *International Journal of Intelligent systems and Applications (IJISA)*, vol. 5, no. 1, pp. 52-58, 2012, https://doi.org/10.5815/ijisa.2013.01.05.

[20] C. Nagarajan, M. Madheswaran and D. Ramasubramanian, "Development of DSP based Robust Control Method for General Resonant Converter Topologies using Transfer Function Model," *Acta Electrotechnica et Informatica Journal*, vol. 13, no. 2, pp. 18-31, 2013, http://www.aei.tuke.sk/papers/2013/2/04_Nagarajan.pdf.

[21] M. Madheswaran and C. Nagarajan, "DSP Based Fuzzy Controller for Series Parallel Resonant converter," *Frontiers of Electrical and Electronic Engineering*, vol. 7, no. 4, pp. 438-446, 2012, https://doi.org/10.1007/s11460-012-0212-0.

[22] K. Umadevi and C. Nagarajan, "Design and implementation of novel soft switching method based DC-DC converter with non-isolated coupled inductor in solar system using FPGA," *Microprocessors and Microsystems*, vol. 73, p. 102952, 2020, https://doi.org/10.1016/j.micpro.2019.102952.

[23] C. Nagarajan and C. Mathiyalagan, "Design and Implementation of Bridgeless Buck Converter with Fuzzy Controller Fed PMDC Drive," *Journal on Soft Computing*, vol. 2, no. 3, pp. 337-340, 2012, https://doi.org/10.21917/ijsc.2012.0052.

[24] C. S. Lakshmi and C. Nagarajan, "Comparison of Shunt Active Filter Controllers for Harmonic Elimination," *Suraj Punj Journal for Multidisciplinary Research*, vol. 11, no. 4, pp. 674- 678, 2021, http://www.spjmr.com/gallery/122spjmr%201491.pdf.

[25] A. Rajavel and N. R. Prabha, "Fuzzy logic controller-based boost and buck-boost converter for maximum power point tracking in solar system," *Transactions of the Institute of Measurement and Control*, vol. 43, no. 4, pp. 945-957, https://doi.org/10.1177%2F0142331220938211.

[26] C. Nagarajan, B. Tharani, S. Saravanan, and R. Prakash, "Performance Estimation and Control Analysis of AC-DC/DC-DC Hybrid Multi-Port Intelligent Controllers Based Power Flow Optimizing Using STEM Strategy and RPFC Technique," *International Journal of Robotics and Control Systems*, vol. 2, no. 1, pp-124-139, 2022, https://doi.org/10.31763/ijrcs.v2i1.562.

[27] C. Nagarajan, B. Tharani, S. Saravanan, and M. Muruganandam, "Performance Analysis of Hybrid Multi-Port AC-DC/DC-DC Embedded Based Energy Flow Optimizing Using Resilient Power Flow Control (RPFC) Technique," *Asian Journal of Electrical Sciences*, vol. 10, no 2, pp-16 -28, 2021, https://doi.org/10.51983/ajes-2021.10.2.3039.

[28] S. Sreejith, I. Gandhi, D. Samiappan, and M. Muruganandam, "Security Constraint Unit Commitment on Combined Solar Thermal Generating Units using ABC Algorithm," *International Journal of Renewable Energy Research*, vol. 6, no. 4, pp. 1361-1372, 2016, https://doi.org/10.20508/ijrer.v6i4.4559.g6925

[29] M. Muruganandam and M. Madheswaran, "Experimental verification of chopper fed DC series motor with ANN controller," *Frontiers of Electrical and Electronic Engineering*, vol. 7, pp 477-489, 2012, https://doi.org/10.1007/s11460-012-0211-1.

[30] M. Muruganandam, I. Thangaraju, and M. Madheswaran, “Simulation and Implementation of an Embedded Hybrid Fuzzy Trained Artificial Neural Network Controller for Different DC Motor,” *International Journal of Engineering and Technology*, vol. 6, no. 1, pp. 315-332, 2014, https://www.enggjournals.com/ijet/docs/IJET14-06-01-370.pdf.